nature catalysis

Review article

https://doi.org/10.1038/s41929-024-01115-6

Lithium-mediated nitrogen reduction to ammonia via the catalytic solid–electrolyte interphase

Received: 17 October 2023

Accepted: 23 January 2024

Published online: 11 March 2024

Check for updates

Wesley Chang[1,2], Anukta Jain[1,2], Fateme Rezaie[1] & Karthish Manthiram[1]

The lithium-mediated nitrogen reduction reaction (LiNRR) produces ammonia in ambient conditions. This electrochemical pathway is dependent on a catalytic solid–electrolyte interphase—a nanoscale passivation layer formed from reductive electrolyte decomposition on the surface of lithium metal. The catalytic solid–electrolyte interphase is a unique nanostructured environment that exists on reactive metal surfaces and intimately influences product selectivity. Here we explore recent progress made in the field of lithium-mediated nitrogen reduction to ammonia, especially in light of growing knowledge about the nature of the catalytic solid–electrolyte interphase. We systematically analyse the observed chemical species and reactions that occur within the solid–electrolyte interphase. We also summarize key developments in kinetic and transport models, as well as highlight the cathodic and complementary anodic reactions. Trends in ammonia selectivities and rates with varying electrolyte compositions, cell designs and operating conditions are extracted and used to articulate a path forward for continued development of lithium-mediated nitrogen reduction to ammonia.

Dinitrogen (N_2) is an inert gas molecule under ambient conditions (25 °C, 1 bar) because of its strong covalent triple bond (bond dissociation energy of 960 kJ mol^{-1}) and the absence of a permanent dipole[1]. For this reason, the conventional Haber–Bosch process for nitrogen fixation to produce ammonia requires temperatures of at least 400 °C and pressures of at least 200 bar (ref. 2). Biological nitrogen fixation to synthesize ammonia under ambient conditions occurs in the nitrogenase enzyme, which polarizes the N_2 molecule and breaks its triple bond through adenosine triphosphate (ATP) hydrolysis[3,4]. Inspired by nitrogenase, homogeneous molecular catalysts, which can coordinate nitrogen and turn it into a redox-active ligand, have been developed for ammonia synthesis at ambient conditions and with comparable selectivities[5–7]. However, the only process at ambient conditions by which N_2 reduction to ammonia has been verified to occur at commercially promising rates and efficiencies of almost 100% is through the heterogeneous, electrochemical lithium-mediated nitrogen reduction reaction (LiNRR)[8,9]. Lithium metal can dissociate nitrogen under ambient conditions, and its high enthalpy of hydration coupled with its small nucleus make it the strongest reducing agent of all metals (−3.04 V versus standard hydrogen electrode, SHE)[10]. Other alkali metals, with similarly negative reduction potentials, can dissociate nitrogen but do not form stable nitrides under ambient conditions[11,12]. Electrodeposition of lithium metal occurs in non-aqueous and aprotic electrolytes, which are thermodynamically unstable in the presence of lithium metal, but kinetically stable due to the formation of a surface passivation layer[13]. This surface film, called the solid–electrolyte interphase (SEI), mitigates further reactions between the metallic lithium and the electrolyte, and has played a key role in the development of commercial lithium batteries. For example, the phenomenon of SEI formation on graphitic carbons led to the commercialization of the lithium-ion battery because of its ability to stabilize the electrode, despite operation at potentials outside the thermodynamically stable

[1]Division of Chemistry and Chemical Engineering, Caltech, Pasadena, CA, USA. [2]These authors contributed equally: Wesley Chang, Anukta Jain.
e-mail: karthish@caltech.edu

range of the electrolyte[14]. LiNRR leverages this half century of research and the development of rechargeable lithium-metal batteries, including non-aqueous electrolyte design, interphase engineering and related methods of characterization. There have been several reports using aqueous lithium-based electrolytes for ammonia synthesis, but, given the absence of lithium-metal deposition at relevant reductive potentials (below −3.04 V versus SHE), these results and proposed mechanisms require further verification[15,16].

LiNRR for electrochemical ammonia synthesis is unique as a catalytic process because N_2 reduction and protonation are dependent on and occur within this SEI layer, which plays a key role in mediating catalysis. In this system, the electrochemical deposition of metallic lithium in the presence of nitrogen gas forms lithium nitride, which reacts with available protons to produce ammonia (Fig. 1a,b). These reactions can occur in two different types of electrochemical cells: batch cells and flow cells. A batch cell is a closed system in which all reactants are combined in a single-compartment cell, and the products remain inside this closed system. Examples of batch cells used in LiNRR are autoclaves, which can access elevated pressures, and glass cells, which operate under ambient conditions (Fig. 1c). A flow cell, on the other hand, is an open system where all or some of the reactants (electrolyte or gas) continuously flow through the cell. In the LiNRR field, flow cells include parallel-plate cells, which separate the anode and cathode in fixed geometries and in separate compartments, and in which nitrogen gas flows through the electrolyte, and gas diffusion electrode (GDE) cells, which incorporate defined flow paths for the gaseous reactant to contact the electrolyte through a porous medium (Fig. 1c). In LiNRR, the fraction of total charge passed that leads to ammonia production, as opposed to alternative outcomes such as SEI formation, excess lithium deposition or hydrogen evolution, is termed the ammonia Faradaic efficiency (FE).

The history of LiNRR starts in the 1930s with a pioneering report by Fichter et al. on stepwise lithium plating, nitridation and protolysis in alcohol-based electrolytes at elevated pressures[17]. Within an autoclave-type electrolysis cell, an initial current of 0.5 A was applied to deposit lithium metal for 5 h. The lithium was electrodeposited in an electrolyte comprising lithium chloride in ethanol. Although negligible ammonia was quantified at atmospheric pressure, the FE increased by up to 10% at an extraordinarily high pressure of 1,000 bar. It was hypothesized that the low ammonia selectivity could be due to the formation of a surface coating on the electrode, a half century before a more specific articulation of the nature of the SEI in lithium-metal batteries[14]. LiNRR was then revisited in the 1990s by Tsuneto and colleagues (Fig. 1d)[18,19]. They reported the first instance of using tetrahydrofuran (THF) as the electrolyte solvent in LiNRR. The experiments were carried out in a single-compartment autoclave cell, wherein lithium metal was plated onto a copper electrode using a 0.2 M lithium perchlorate, 1% ethanol in THF electrolyte. Nitrogen gas at 50 bar was used to produce ammonia with an FE of 48.7%. Further efforts to screen for different working-electrode metals, lithium salts and proton-donor additives were employed, with the most optimized set of experimental conditions resulting in an FE of 59.8%. In 2017, McEnaney and colleagues developed a three-step strategy to separate the electrolysis, nitridation and protonation reactions to achieve 88.5% FE towards ammonia, albeit in a manner that involved solids handling, transfer between different vessels and high temperatures[20]. LiOH was first electrolysed at 450 °C, then the molten salt was exposed to nitrogen gas at temperatures of up to 100 °C. Finally, the lithium nitride was subjected to an exothermic reaction with water to produce ammonia. Unlike a continuous process, batch processes require additional separation and purification steps, as well as the need for a large lithium source, which may increase system cost and complexity. Several industry efforts were patented between 2010 and 2015, claiming various iterations of electrochemical ammonia synthesis using materials including molten salt electrolytes at higher temperatures and lithium-ion conductive membranes[21,22].

In 2019, Lazouski and colleagues developed a strategy to produce ammonia under ambient conditions by flowing nitrogen gas through a two-compartment parallel-plate flow cell[8]. A combined transport-kinetic model was developed based on experimental results, describing the key mechanistic steps of the process[8]. The major contributions of this work were to identify the transport of nitrogen as a rate-limiting step at high current densities, in addition to using $^{15}N_2$ isotopic labelling to verify the production of ammonia from nitrogen reduction. Andersen et al. also proposed a rigorous quantitative isotope measurement protocol to prevent false-positive results[9]. A major contribution of this work was addressing why isotope labelling experiments were insufficient to unambiguously confirm the origin of ammonia stemming from nitrogen reduction. According to the authors, recent studies utilizing isotope labelling lacked quantitative data and did not meet their protocol requirements, which included assessing the purity of $^{15}N_2$ gas and ensuring the repeatability of quantitative $^{15}N_2$ experiments. In 2020, Lazouski and colleagues devised a GDE cell to overcome the transport limitations of N_2 gas in non-aqueous electrolytes[23]. A platinum on stainless-steel cloth (Pt/SSC) GDE was implemented for the hydrogen oxidation reaction (HOR) at the anode, overcoming the problem of undesired solvent and proton-donor oxidation at the anode. An electrochemical Haber–Bosch reactor was also developed that coupled a water electrolyser (to supply hydrogen gas) to the four-compartment GDE cell, producing ammonia from N_2 and H_2 under ambient conditions. Between 2020 and 2022, other methods were developed, including a potential cycling strategy to improve stability, the use of porous copper electrodes to increase the electrochemical surface area, and a phosphonium-ion proton carrier to overcome the limitations of a sacrificial source of protons in this system[24–26]. Steady improvements in rates of up to 1 A cm^{-2}, selectivities up to 99% at 15 bar, and energy efficiencies up to 14% have begun to improve the metrics associated with lithium-mediated ammonia synthesis[25,27,28].

In this Review we highlight key themes across different electrolyte compositions, cell designs and cell operating parameters that drive ammonia selectivity and rates. We first discuss the common themes in SEI chemistry and structure, with respect to the different electrolyte salts, solvents and proton donors that have been reported. We discuss these themes in the context of lessons learned from electrolyte engineering of rechargeable batteries, finding commonalities in SEI structure and function, yet important differences between battery SEI and catalytic LiNRR SEI layers. We also touch on the various characterization techniques used for elucidating the nanoscale structure of the SEI. Because the catalytic SEI is crucial for controlling the kinetics and transport of this system, we compare similarities and differences among the various kinetic and transport models developed in this field. After a review of the electrode and interfacial effects, we zoom out and focus on cell-level aspects. Several recent articles have summarized key advancements in electrocatalytic N_2 reduction, including the genuine verification of N_2 activation[29–32]. Common to all studies is the importance of accurate detection and quantification of ammonia species, which has been comprehensively summarized in other studies and will not be a focus here[33–44]. If proven beyond the academic research laboratory, LiNRR could enable modular and distributed ammonia generation at point of use, overcoming the use of high temperatures (350–500 °C) to improve the kinetics and high pressures (150 to 300 bar) to improve the thermodynamics in the conventional Haber–Bosch process[2,45,46]. However, substantial advances in our fundamental understanding and systems engineering are needed to increase the rate, selectivity and energy efficiency of the process before commercialization.

Nitrogen reduction within catalytic SEIs

The SEI formed from non-aqueous electrolyte decomposition on metallic lithium is a complex structure composed of both inorganic and organic compounds (Fig. 2). The existence of this SEI allows for electrochemical cell operation, despite lithium plating potentials being

https://doi.org/10.1038/s41929-024-01115-6

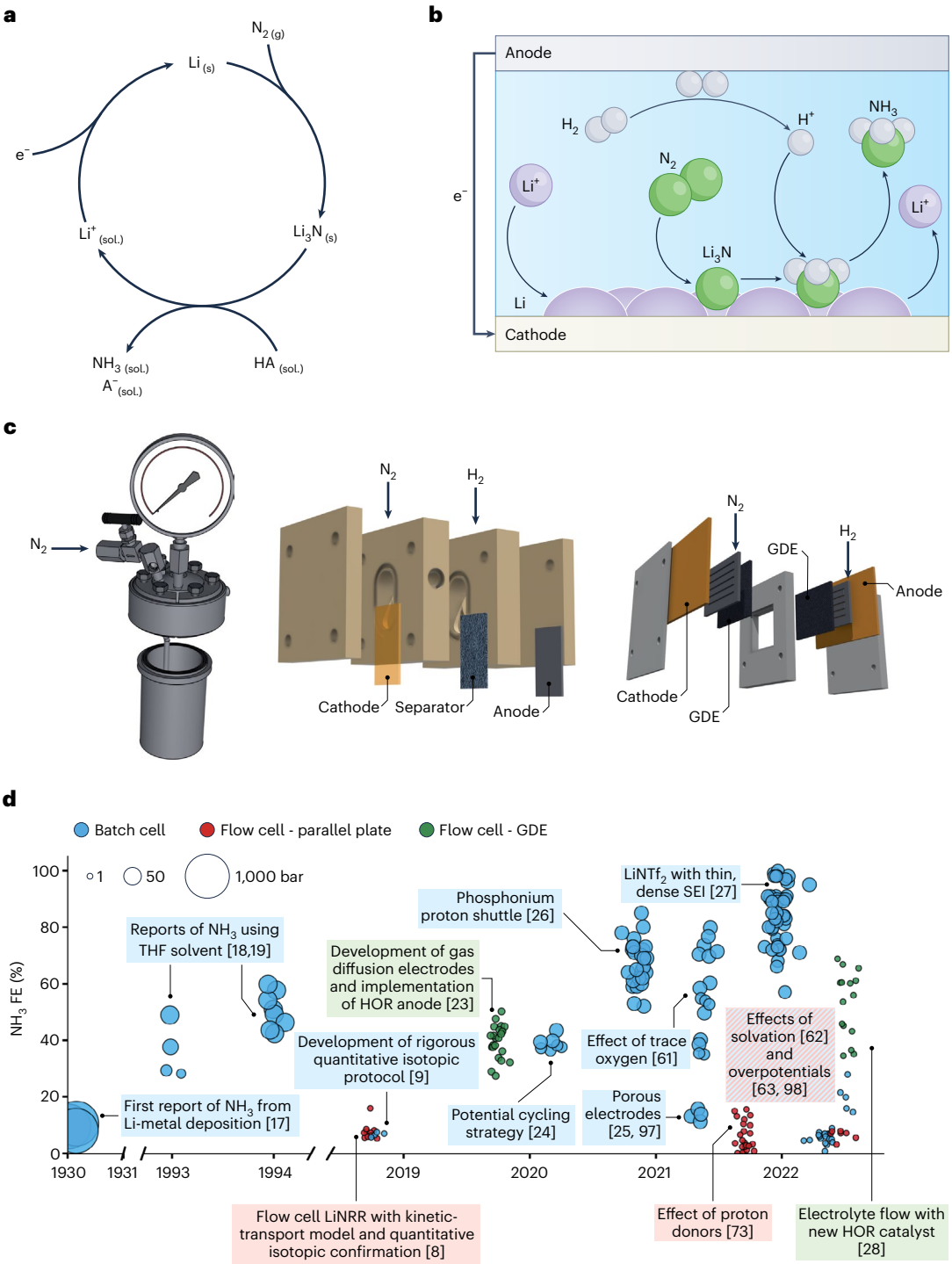

Fig. 1 | Overview and history of LiNRR. a, Schematic of the LiNRR cycle, where (sol.) indicates a solution, (s) indicates a solid and (g) a gas. **b**, Schematic of the cathode and anode reactions. **c**, LiNRR is conducted in a single-compartment batch cell, a parallel-plate flow cell or a GDE flow cell (with flow of electrolyte, gas or both). **d**, Ammonia FEs in published data under optimized conditions for LiNRR. Colour indicates the type of cell (batch cell, parallel-plate flow cell, GDE flow cell) and marker size indicates the relative nitrogen pressure (bar). Text labels indicate key advancements made along with references[8,9,17–19,23–28,61–63,73,97,98]. All data are taken from the cited literature and their respective supplementary information. Data-processing scripts were written in Python and are hosted, open source, on GitHub[99].

outside the thermodynamically stable voltage window of the electrolytes used[14,47,48]. The SEI on graphitic carbons and metallic lithium kinetically enabled reversible lithium-ion intercalation and metal deposition, respectively, despite the associated thermodynamic challenge[49–51]. For those interested in the interplay of SEIs and lithium-battery electrolyte chemistry, we refer the reader to several exhaustive publications[49,52,53].

Productively harnessing the SEI to encourage catalytic steps involved in LiNRR entails understanding and designing this reactive microstructural interphase, which is differentiated from the bulk metal electrode and the bulk liquid electrolyte, in strong contrast with conventional electrocatalysis on discrete surfaces at liquid–solid interfaces. The structure and function of the SEI layer depends on the

https://doi.org/10.1038/s41929-024-01115-6

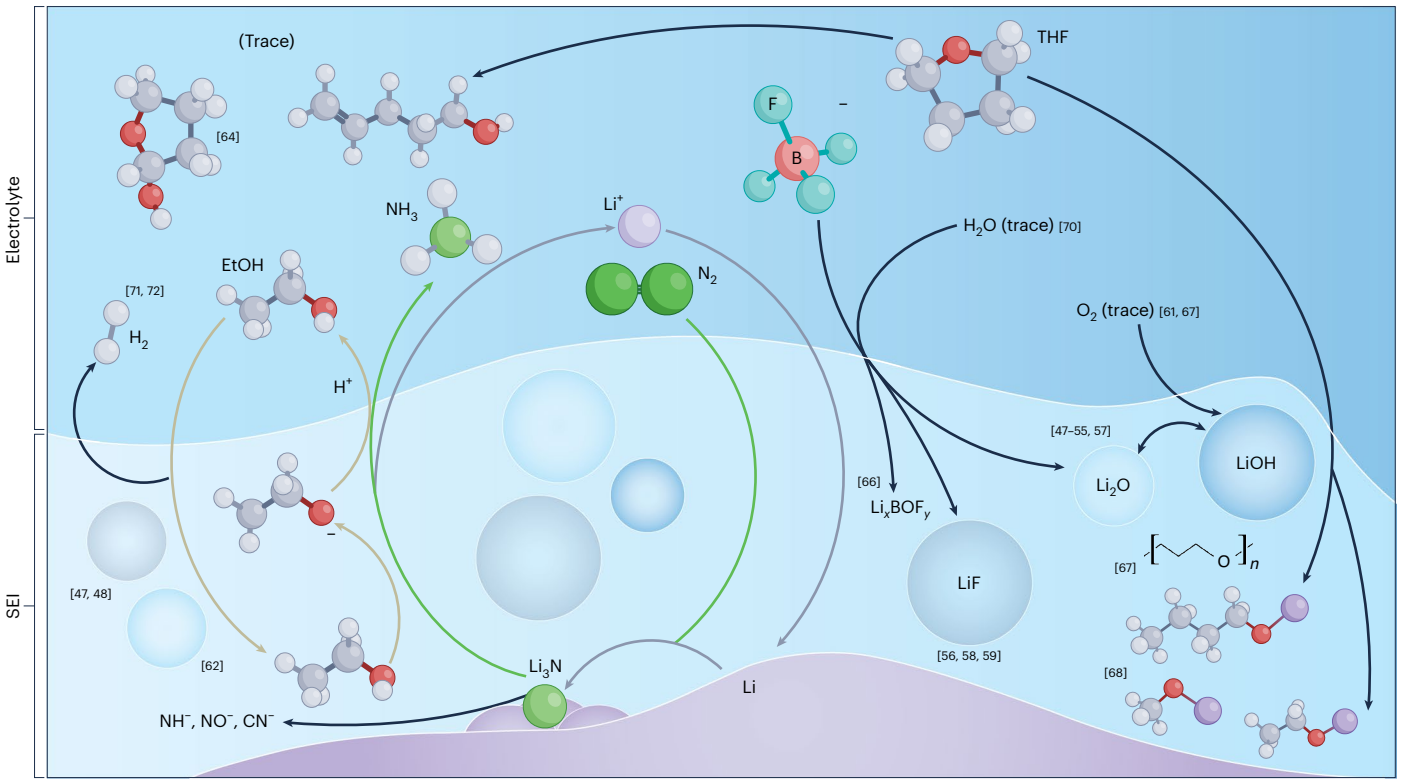

Fig. 2 | Reaction network governing LiNRR conducted in THF with $LiBF_4$ and ethanol. Orange arrows denote the proton cycle, green arrows the nitrogen cycle, and grey arrows the lithium cycle. Relevant literature references have been included next to their appropriate reactions in the figure. The citations refer to studies in which these reactions were observed, and include electrolyte solvent (THF) oxidation reactions, the parasitic hydrogen evolution reaction, SEI-forming reactions from electrolyte salt reduction, SEI-forming reactions from electrolyte solvent breakdown, reactions with trace moisture or oxygen contaminants, and reactions involving nitrogen.

choice of electrolyte. The stable electrolyte salts for lithium electrochemistry initially used included lithium perchlorate ($LiClO_4$), lithium tetrafluoroborate ($LiBF_4$) and lithium hexafluoroarsenate ($LiAsF_6$), with THF and propylene carbonate (PC) solvents. However, the poisonous nature of $LiAsF_6$, explosive risk of $LiClO_4$ and poor conductivity of $LiBF_4$ led to the eventual use of different salts, including lithium hexafluorophosphate ($LiPF_6$), lithium bis(fluorosulfonyl)imide (LiFSI), lithium bis(trifluoromethane)sulfonimide (LiTFSI, also abbreviated as $LiNTf_2$) and lithium difluoro(oxalato)borate (LiDFOB)[54,55]. Out of these working electrolyte salts, LiNRR studies have primarily used $LiClO_4$, $LiBF_4$ and $LiNTf_2$.

Inorganic constituents of the SEI

In LiNRR, the presence of nitrogen and protons leads to a distinct SEI structure and chemistry compared to the conventional electrolytes used in lithium-ion and lithium-metal batteries. The lattice spacings of the polycrystalline inorganic regions formed in the SEI with $LiBF_4$ electrolyte salt in THF, with and without ethanol, are consistent with the presence of LiOH and LiF compounds, as determined by X-ray photoelectron spectroscopy (XPS) and cryogenic transmission electron microscopy (cryo-TEM)[56]. Li and colleagues speculated that the low lithium surface mobility and the electronically insulating properties of LiF may deter excess lithium plating in favour of lithium nitridation and thus favour subsequent ammonia production[25]. These results echo the initial characterization studies on $LiBF_4$-based electrolytes for lithium-metal batteries. Using XPS, Kanamura and colleagues found that the SEI formed in the presence of $LiBF_4$ in THF to consist of LiF and other organic compounds[57]. They speculated that this LiF-containing SEI layer might have a porosity that varied over time due to reactions with Li_2CO_3 or LiOH, as evidenced by changing resistance measurements. Furthermore, modern characterization techniques have found that electrolytes that improve battery performance are rich in LiF from anion reduction[58,59]. Before adaptation for LiNRR electrode characterization, cryo-TEM was used to reveal inorganic crystalline grains dispersed throughout an amorphous layer in battery SEIs[60]. Therefore, an SEI with LiF as an inorganic species is observed not only in lithium-metal battery electrolytes ($LiBF_4$ in THF)[57], but also in the electrolytes used for LiNRR ($LiBF_4$ in THF with ethanol)[56]. Replacing $LiBF_4$ salt with $LiNTf_2$ in THF and ethanol also results in a LiF-containing SEI, as characterized by XPS and X-ray diffraction (XRD)[27]. Furthermore, $LiNTf_2$ in THF and ethanol generally results in even higher rates and selectivities than when $LiBF_4$ is used as the electrolyte salt (Fig. 3).

Although lithium fluoride-containing SEIs have been widely observed and point to shared SEI characteristics between lithium batteries and LiNRR, lithium fluoride in the SEI is neither sufficient nor necessary for ammonia synthesis. This can be established by examining the fluoride-free systems that have been investigated for LiNRR, which perform reasonably well, as well as fluoride-containing systems, which do not perform well for LiNRR. In their seminal study, Fichter and colleagues used LiCl and LiBr in pure ethanol, a system that did not contain any fluoride, and were the first to establish that LiNRR is feasible[17]. Tsuneto and colleagues used non-fluorinated $LiClO_4$ salt with THF and ethanol and obtained over 50% FE, albeit at a high pressure of 50 bar (refs. 18,19). Since then, many other studies have used $LiClO_4$ as the electrolyte salt for LiNRR and have reported high production rates and FEs for ammonia[25,61–65]. XPS characterization describes the resulting SEI as rich in inorganic chloride species from perchlorate salt decomposition[62]. An optimal salt concentration of 0.6 M was observed, which is speculated to result from competition between increasing favourable inorganic SEI species and decreasing nitrogen-gas solubility and

https://doi.org/10.1038/s41929-024-01115-6

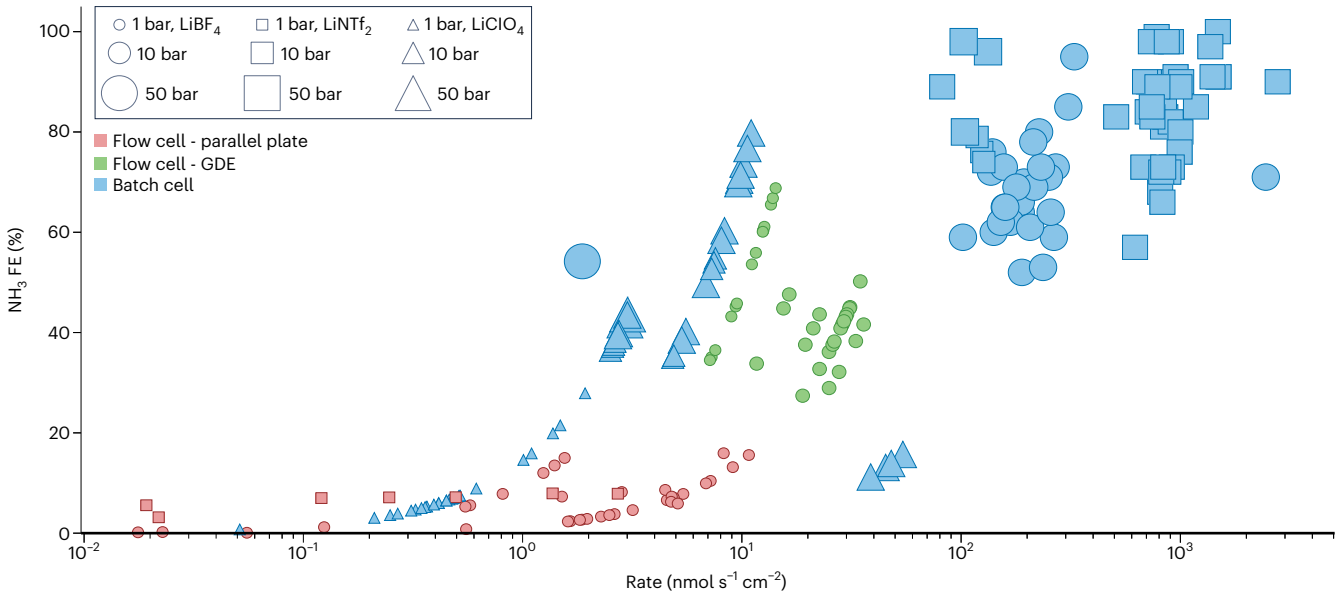

Fig. 3 | Comparison of selectivity and rate across different electrolyte salts and cell form factors. Marker colours indicate cell type, marker shape indicates electrolyte salt type, and marker size indicates N_2 pressure. Autoclaves and glass cells (blue) generally exhibit higher rates of ammonia production, probably due to the increased accessibility of active electrode sites. $LiNTf_2$, which has primarily been investigated in reports using autoclaves and glass cells, exhibits the fastest rates of ammonia production, followed by $LiBF_4$ and then $LiClO_4$. This figure depicts a comprehensive set of available published data for three main salts: $LiNTf_2$, $LiBF_4$ and $LiClO_4$. All data are taken from cited literature (the same data as shown in Fig. 1d) and their respective supplementary information. Data-processing scripts were written in Python and are hosted, open source, on GitHub[99].

diffusion[62]. In addition, $LiPF_6$, which does form a LiF-abundant SEI, does not produce substantial amounts of ammonia. Hence, although lithium fluoride is observed in many of the SEIs that perform favourably for LiNRR, its presence does not guarantee that ammonia is synthesized.

The fact that there is not a clear connection between lithium halide content in the SEI and ammonia selectivity may originate from the effects of other inorganic compounds in the SEI. For example, the decomposition of $LiBF_4$ to LiF necessarily involves the generation of additional products containing boron, such as Li_xBOF_y, which has been extensively documented in lithium-metal battery research but not analysed in LiNRR studies[66]. In $LiNTf_2$ salt-based electrolytes, reduced inorganic S–O species were detected by XPS, and in $LiClO_4$ salt-based electrolytes, inorganic chloride species were detected in the SEI by XPS[27]. The effects of these S–O and chloride species on lithium deposition, nitridation and protonation are not yet understood, further emphasizing that LiF is just one part of a more complex set of SEI constituents. Furthermore, the Li_3N intermediate is rarely detected by either XPS or cryo-TEM, and is thought to be a short-lived species in the SEI[56]. Westhead and colleagues also detected no nitrogen-containing species in N 1*s* XPS, and only observed three nitrogen-containing species in time-of-flight secondary ion mass spectrometry (ToF-SIMS), namely NH^-, NO^- and CN^- (Fig. 2)[62].

Organic constituents of the SEI

Beyond the crystalline inorganic components of the SEI discussed above, there are several amorphous organic constituents of the SEI resulting from solvent decomposition. XPS and cryo-TEM reveal that, in the absence of ethanol, THF-breakdown products, such as lithium butoxide and other polyTHF compounds, are prevalent in the SEI[56]. Following the addition of ethanol, the oxygen–carbon ratio in surface species increases and the O 1*s* C–O intensity widens, implying an increase in ethanol-breakdown products, which are organic species with shorter carbon chains and more diverse oxygen-containing compounds such as lithium ethoxide[56]. These ethanol-rich breakdown products were also detected by ^{1}H NMR spectroscopy when samples were prepared by dissolving solid lithium deposits in D_2O and $CDCl_3$ solvents (Fig. 2)[67]. In previous literature on THF-based battery electrolytes, Aurbach and colleagues used Fourier-transform infrared spectroscopy and gas chromatography (GC) to also observe the presence of lithium butoxide in the SEI[68]. Aside from insoluble solid products, there are also soluble organic decomposition products within the electrolyte; these are detected by GC coupled with mass spectrometry (GC-MS). Examples include (2,5 or 2,3)-dihydrofuran, but-(2 or 3)-enal, 4-hydroxybutanal or tetrahydrofuran-2-ol, and succinaldehyde, albeit at concentrations less than 100 ppm (ref. 64).

Effects of additives on the SEI

Several studies have investigated the effects of adding trace concentrations of water and oxygen to the electrolyte. This alters the relative ratios of inorganic oxides and fluorides in the SEI. Li and colleagues found that 0.8 mol% oxygen content maximizes the ammonia FE (Fig. 1d). They attributed this result to decreased electrolyte decomposition by-products, as measured by GC-MS and NMR spectroscopy, while maintaining the availability of H^+ and N_2 at the lithium surface[61,67]. The FE increases proportionately with the partial pressure of oxygen gas (peak behaviour is observed between 0.5 and 0.8 mol% O_2 in N_2 at 20 bar, and between 1.2 and 1.6 mol% O_2 in N_2 at 10 bar) and decreases with higher O_2 content, which was attributed to an increase in H_2O in the electrolyte and a subsequent oxygen reduction reaction (ORR) at the cathode. It was speculated that the increase in Li_2O content forms a more homogeneous and uniform SEI, which may slow Li^+ diffusion and lead to more uniform plating, as has been reported previously for non-aqueous lithium–air batteries[69]. Additionally, the increase in oxide content was also attributed to a decreased rate of electrolyte degradation, which was observed by monitoring the working-electrode potential and calculating the time taken for it to change by 1 V during chronopotentiometry with potential cycling. In a similar vein, Spry and colleagues attribute ammonia FE improvements to trace concentrations (40 mM) of water leading to Li_2O formation in the SEI[70]. The attribution of trace water effects on Li_2O in this case, but on LiF in other cases, is another indicator that the effect of individual SEI components on LiNRR is poorly understood.

Proton donor and bulk electrolyte property effects on the SEI

The availability of protons in LiNRR is a double-edged sword. A sufficient ethanol concentration is required to drive protonation of Li_3N, but ethanol also reacts with lithium metal to form lithium ethoxide and hydrogen gas[71,72]. A wide range of other proton-donor classes were tested, including linear and branched aliphatic alcohols, ether alcohols and unsaturated alcohols, with the linear aliphatic alcohols such as ethanol and butanol presenting the highest FEs (Fig. 1d)[73]. Ethanol has been used as the proton-donor source and the proton carrier in the vast majority of LiNRR studies. The impact of this proton donor on the SEI was studied by Steinberg and colleagues, who discovered that, although it may appear that the reaction of lithium and nitrogen to form lithium nitride does not involve ethanol, the presence of the proton donor is necessary for lithium nitridation[56]. If ethanol is removed from the electrolyte while keeping all other components constant, lithium metal accumulates on the surface rather than lithium nitride, with a thin, conformal and passivating SEI that is rich in BF_4^- and THF decomposition products forming on the surface of the lithium, as observed by cryo-TEM. It is likely that this SEI is preventing access of nitrogen to the underlying lithium metal. In contrast, once the proton donor is added, cryo-TEM reveals that this passivating SEI gives way to a porous and fractured SEI. Several reasons for this have been suggested. The reaction of ethanol with lithium metal to form hydrogen gas could result in a physical attack on the SEI, reducing its mechanical stability. The formation of ethoxide via the same reaction could also lead to a more permeable SEI to nitrogen gas, as the SEI could swell in the presence of increased organic products in the electrolyte and thus bring dissolved nitrogen closer to the surface lithium. Furthermore, ethanol and ethanol-derived products could chemically react with the SEI and improve lithium–nitrogen reactivity[56]. As well as alcoholic proton donors, an ionic liquid-phosphonium proton carrier (phosphonium tris(pentafluoroethyl)trifluorophosphate salt) was introduced by Zhou[74] and Suryanto[26] and colleagues as an effective proton carrier with high nitrogen solubility. However, the SEI composition of these ionic liquid species has not been characterized.

LiNRR reactions are complex, and the native SEI could be altered by the cell disassembly steps necessitated by ex situ techniques such as XPS and cryo-TEM. Thus, the use of in situ techniques, such as NMR spectroscopy[75] and an electrochemical quartz-crystal microbalance[76], to measure changes in the SEI during electrochemical testing may help to understand open questions surrounding the SEI in LiNRR. For example, Blair and colleagues used synchrotron neutron reflectometry to measure the changing lithium layer in situ, and found that switching back to open-circuit voltage (OCV) reduces the thickness of the lithium layer[77]. This implies that corrosion processes that consume lithium metal, such as solvent decomposition and ammonia production, may occur during OCV. This was also observed in the potential cycling protocol developed by Andersen and others[24]. All LiNRR studies with reported FEs towards ammonia have used THF—a cyclic ether—as the solvent. Other classes of solvent, such as carbonates or linear ethers, have not demonstrated ammonia production, and the reasons remain unknown. A better understanding of how solvent identity and structure impacts catalytic SEI chemistry may be informative[78–80].

Kinetic and transport models

Theoretical models have played an important role in deconvoluting the complex structure and dynamic nature of the catalytic SEI, bringing meaning to many of the experimental results described above.

Transport models

A key role of the SEI is to deliver nitrogen and protons to the metallic lithium surface, and to mitigate unfavourable side reactions. In this vein, controlling the transport of competing species, not just through the SEI but through the electrolyte beyond it, is key to Faradaically selective LiNRR. Based on the observation of a plateau in partial current for ammonia with increasing overall current density, Lazouski and colleagues hypothesized that nitrogen transport to the electrode may be rate-limiting[8,18,24]. The limiting current density for nitrogen reduction in this system (11.6 ± 8.0 mA cm^{-2}) was calculated using values for nitrogen diffusivity and solubility in THF[78,81]. Additionally, the thickness of the boundary layer formed at the SEI (50 ± 15 μm) was estimated from a limiting current-density analysis on ferrocenium hexafluorophosphate reduction[82,83]. These parameters were used to predict a transport-limited current density for ammonia. Accordingly, a transport model was developed that suggests that fast mass transport of nitrogen is critical to obtaining high ammonia FEs, and the partial current density towards ammonia (1.3 ± 0.3 mA cm^{-2}) is only one-third of the predicted transport-limited current density (3.9 ± 0.9 mA cm^{-2})[84]. Based on this model, Lazouski and colleagues proposed that decreasing the boundary-layer thickness for nitrogen diffusion could increase this partial current density[23]. The use of SSC as the GDE in these non-aqueous electrolyte systems achieves this purpose by creating a thin electrolyte layer that is in intimate contact with the catalyst surface and through which the nitrogen gas must now diffuse instead of through the entire bulk electrolyte. Electrolyte penetration and flooding into the GDE is prevented by establishing a positive pressure gradient across the SSC with the use of a water column attached to the outlet of the gas compartment in the three-compartment cell set-up. This pressure gradient across the SSC can be tuned to change the direction of gas flow—either through the electrode to saturate the electrolyte (defined as the Laplace pressure), or past the electrode. An increased partial current density for ammonia (8.8 ± 1.4 mA cm^{-2}) at an FE of $35.6 \pm 6\%$ was obtained; an even higher FE of up to $47.5 \pm 4\%$ could be obtained when the FE was optimized for partial current density. Visualization of the ammonia selectivity and the rates for all published data indicate that GDE cells (Fig. 3, green) show markedly improved rates and selectivities compared with their parallel-plate cell counterparts, which use planar electrodes (Fig. 3, red) at identical pressures.

In addition to considering the transport of nitrogen to the electrode surface, one can also consider the rates of diffusion of Li^+ and H^+ from the bulk solution to the surface of the lithium metal. An ideal ratio of nitrogen to proton molar flux through the electrolyte and SEI was determined by Andersen and colleagues to be 1:6 based on the species balance under steady-state conditions[24]. The model suggests that these diffusion rates should not be substantially lower than the rate of lithium deposition if high FEs for ammonia are to be obtained[24]. If the rate of lithium deposition results in excess lithium plating beyond the achievable rates for nitridation and protonation, a subsequent OCV rest period may allow the excess lithium metal to undergo the necessary thermochemical steps for ammonia production (Fig. 1a). In this vein, Andersen and colleagues developed a transient potential cycling protocol involving short deposition pulses of 1 min at −2 mA cm^{-2} followed by a subsequent OCV rest step lasting between 3 and 8 min (ref. 24). Continued ammonia production during OCV was verified using electron-ionization mass spectrometry[42].

Kinetic models

Nitrogen and proton transport through the SEI is essential for LiNRR, but one must also consider the kinetic parameters that govern the reaction rates of the lithium deposition, nitridation and protonation reactions. To model these reactions, kinetic models assume a constant surface concentration of metallic lithium, by invoking a quasi-steady-state approximation[8,24,73]. Lazouski and colleagues proposed a kinetic model that identified lithium nitridation to generate ammonia, and lithium protonation to generate hydrogen, as the two main rate-limiting reactions that govern selectivity towards ammonia versus hydrogen. The rate constants of these thermochemical reactions are assumed to be independent of the operating electrochemical conditions. The kinetic model showed that nitridation, which leads to ammonia, is first order in nitrogen, and protonation, which leads

to hydrogen, is first order in ethanol concentration, based on experimental results. However, the orders with respect to lithium differ for the two reactions[8,73]. Nitridation has a higher order dependence on lithium compared to protonation, and the peak behaviour in FE is attributed to increased competition by direct lithium protonation at high proton-donor concentrations (>0.1 M). This causes a reduction in the amount of lithium available for nitridation and thus for subsequent ammonia synthesis. This kinetic model was coupled to the transport model[8] described above to account for nitrogen depletion effects. The assumptions made in this kinetic model, however, cannot accurately determine the distribution of FE towards other reactions, such as electrolyte decomposition and excess lithium plating, nor capture the influence of the SEI on interfacial kinetics.

According to the kinetic model proposed by Andersen and colleagues, nitrogen dissociation on metallic lithium at the cathode is assumed to be a kinetically facile and irreversible reaction at room temperature, with a low calculated effective activation-energy barrier[20,24]. Singh and colleagues proposed a microkinetic model to predict the nitrogen reduction activity and selectivity for a range of proton-donor concentrations in non-aqueous electrolytes, showing that the low proton activity leads to reasonable ammonia selectivities over those of aqueous electrolytes, but without considering SEI effects[85]. Further development of a microkinetic model could account for a more diverse array of variables known to affect the relevant activation energies, reaction rates and species transport, such as proton-donor identity, electrolyte conductivity and acid dissociation constants.

Although still rudimentary, these kinetic and transport models lay the foundational groundwork for future models that can more accurately account for the effect of the SEI on ammonia synthesis, because the relationship between nanoscale SEI features and mesoscale SEI properties is still unclear. In many cases, more robust experimental methods will be needed for more accurate measurements. For example, experimental confirmation of these theoretical models across diverse reactors also requires accurate ohmic overpotential corrections (*iR* compensation). *iR* compensation is typically done with reference to a platinum pseudo-reference electrode, though a true non-aqueous reference electrode may be more reliable for accurate measurements of equilibrium potentials and lithium-ion activity coefficients. Accurate experimental measurements that verify robust theoretical models will aid the further development of LiNRR for ammonia synthesis.

Anodic reactions

Although we have focused so far on cathodic nitrogen reduction to ammonia, achieving stable, sustainable and continuous ammonia synthesis also necessitates development of the anodic reaction.

Electrolyte oxidative decomposition

An ideal anode would generate the protons that are ultimately consumed at the cathode through either hydrogen or water oxidation, but electrolyte oxidative decomposition may also occur. Therefore, the stability of the electrolyte components, including the solvent, salt and proton carrier at the anode, is important for the continuous viability of ammonia production[73]. Kim and colleagues used a lithium-ion conducting glass ceramic (LISICON) structure to separate an aqueous anodic electrolyte from the non-aqueous catholyte; this avoids THF solvent oxidation and decomposition on a platinum counter electrode. They also demonstrated a membrane-free approach by using an immiscible aqueous/organic hybrid electrolyte, but the production of ammonia is not continuous, as nitridation takes place separately from lithium deposition[86]. These results are encouraging as they allude to the possibility of LiNRR operating within an aqueous environment, resolving the oxidative decomposition of THF-based electrolytes. It has been hypothesized that tertiary alcohols such as 2,2-diphenylpropan-2-ol could make for better proton carriers than traditional primary and secondary alcohols, because they cannot be oxidized to carbonyl-containing compounds at the anode[73]. Another important consideration is the solubility of the deprotonated form of the proton carrier in the electrolyte. Linear aliphatic alcohol proton donors and carriers result in precipitated alkoxides at the cathode, which are sparingly soluble in traditional non-aqueous electrolyte solvents and thus cannot be completely recycled[73]. The most common non-aqueous electrolyte solvent in LiNRR is THF, which undergoes a ring-opening polymerization reaction upon oxidation. The major decomposition products of the electrolyte from THF oxidation have been characterized at the counter electrode[64]. Unlike ethanol, longer-alkyl-chain alcohols (such as isopropanol) and phosphonium-based proton shuttles tend to be more stable and react less with oxidized THF, as evidenced by ^{1}H NMR spectroscopy[87]. Sazinas and colleagues, along with many other studies, also measured a high counter-electrode overpotential (greater than 2 V versus platinum) attributed to both THF and ethanol oxidation[67].

Hydrogen oxidation reaction

An efficient hydrogen oxidation reaction (HOR) on the anode avoids electrolyte decomposition reactions such as THF polymerization and ethanol oxidation[23]. Therefore, molecular hydrogen as the proton source is preferred in LiNRR. Lazouski and colleagues first used a GDE at the anode to feed hydrogen gas into the cell, providing a sustainable source of protons for ammonia generation. By combining LiNRR and HOR into an electrochemical Haber–Bosch reactor, ammonia was produced from nitrogen and hydrogen under ambient conditions. This was then coupled with a commercial water-splitting electrolysis cell to produce ammonia from an overall reaction including only renewable reactants[23]. It was also observed that ~80% of the labile, alcoholic protons present in ethanol went to ammonia production, despite hydrogen evolution occurring at the cathode, thus demonstrating high proton utilization and the regeneration of the proton carrier via HOR at the anode. Alternatively, a lithium-ion conductive solid electrolyte may allow for water splitting as the anodic reaction[88]. Krempl and colleagues performed cyclic voltammetry studies on a platinum electrode under argon and hydrogen atmospheres to demonstrate that proton-generating anodic reactions such as electrolyte or hydrogen oxidation can lead to continuous acidification of the electrolyte over time, because these protons react with the electrolyte salt or solvent instead of recombining with the deprotonated ethoxide[89]. This is substantiated by the observation that most of the ammonia generated is in the liquid phase as protonated NH_4^+, even though gaseous NH_3 is a volatile compound. This leads to parasitic side reactions with electrolyte components, which could negatively impact SEI formation, structure and reactivity. Using a buffered electrolyte with a stable proton acceptor that can recombine with these newly generated protons may prevent this acidification[89].

Suitable HOR electrocatalysts

Lazouski and colleagues devised an SSC electrodeposited with platinum as a GDE at the anode to oxidize hydrogen with almost 100% FE and a current density of 25 mA cm^{-2}—an order of magnitude higher than with a flooded platinum foil[23]. Hodgetts and colleagues conducted a study on suitable HOR electrocatalysts, using $LiNTf_2$ in THF as the electrolyte[90]. Various carbon-supported metal anodes, including Pt/C, Ni/C, Ru/C, Pd/C, Ir/C, Au/C and PtRu/C, were tested. The results revealed that HOR exhibits low activity in THF due to the rapid poisoning of the catalyst surface and blocking of active sites by irreversible electrolyte-oxidation reactions. Of the tested carbon-supported metal catalysts, PtRu/C exhibited the highest HOR activity, suggesting that Pt alloys may promote hydrogen oxidation in organic solvents, but the exact mechanism is not yet understood. Inspired by these studies, Fu and colleagues introduced a PtAu bimetallic alloy as a HOR electrocatalyst, which showed higher activity and longer stability in THF as compared to the conventional Pt anode surface (Fig. 1d)[28]. This is attributed to the increased Pt oxidation potential in the alloy, and the suppression of oxidized species adsorption by Au. They also confirmed

that hydrogen oxidation can continuously supply protons for ammonia synthesis and verified the recyclability of EtOH as a proton carrier by employing operando MS of deuterium (D_2) oxidation. Enabling a continuous supply of protons in GDE flow cells, as opposed to batch cells, holds promise for facilitating scalability. HOR catalysts that decrease the anodic overpotential and mitigate oxidative decomposition of the electrolyte show encouraging promise towards developing a LiNRR cell optimized on both the cathodic and anodic sides.

Cell design and operating conditions

Cathodic and anodic reactions aside, the design and operating environment of the cell also play important roles in efficient and stable LiNRR.

Batch cells—autoclaves and glass cells

One example of a batch cell is an autoclave, a sealed vessel that can be pressurized and which has high volume-to-surface area ratios. Autoclave cells are common in thermocatalysis, but can also be used for electrocatalysis using electrical feedthroughs. High pressures of over 50 bar can be attained with ease, although fixed electrode designs are more difficult to engineer in an autoclave. Autoclave cells have resulted in the highest rates and selectivities achieved so far (Fig. 3) because of their ability to operate at these elevated pressures, thus overcoming the transport limitation of nitrogen in non-aqueous solvents. For example, using autoclave cells held at 15 bar, Du and colleagues achieved nearly 100% FE with a 2 M $LiNTf_2$ electrolyte salt (Fig. 1d)[27]. In another study, Li and colleagues used a single-compartment glass cell placed inside an autoclave, with 0.2 cm^2 to 1 cm^2 geometric area stainless-steel mesh pieces with porous copper deposited on them as the working electrodes[25]. This autoclave cell design was also used by them in their study of trace oxygen content and its effect on the SEI, with the working and counter electrodes placed ~0.5 cm apart, and with surface areas of ~1.8 cm^2. These are approximate values, because the electrodes are dangling in an open container, and the electrode gap is much larger than in an optimized two-compartment parallel-plate flow cell[61]. Another type of batch cell is a glass cell, where high pressures cannot be achieved. Westhead and colleagues conducted LiNRR using a simple glass cell as typically used for laboratory electrochemistry, with electrodes ~1 cm apart and with an electrolyte volume of ~11–15 ml (ref. 62). Glass and autoclave cells are simple to use for initial electrochemical testing but are unlikely to be industrially relevant cell designs, as scaling up production in these batch reactors is challenging due to the substantial interelectrode gap.

Parallel-plate flow cells

Parallel-plate flow cells are electrochemical cells with fixed electrode geometries, typically planar foils, that can have individual compartments for the catholyte and the anolyte, or only one compartment for the entire electrolyte. These cells also contain fixed inlets and outlets for gas and electrolyte flow. As a result of these fixed geometries, less electrolyte volume is used per electrode area compared to autoclave and glass cells. In developing continuous LiNRR, Lazouski and colleagues used a two-compartment parallel-plate cell with a copper-foil cathode and platinum-foil anode separated by a polyethylene based Daramic separator[8]. O-rings were used to compress and seal the cell, which had inlet and outlet ports for the transfer of feed gas. This parallel-plate flow cell design was adapted from the CO_2 electrocatalysis literature[91]. As an alternative to O-rings, gaskets can also be used to ensure effective sealing[92]. For LiNRR, all cell materials should be inert with respect to organic solvents such as THF. This type of cell reduces electrolyte resistance compared to batch cells, where resistance is directly related to the interelectrode distance. This reduction in resistance facilitates the use of higher currents and lower concentrations of supporting electrolyte[93].

GDE flow cells

Although the high rates and selectivities achieved in autoclave cells have not been achieved in parallel-plate flow cells, improvements in cell design have increased the transport-limited current density. As has been the case in the CO_2-reduction literature, GDEs increase the rate of transport of gas to the electrode surface, but also increase system design complexity[23,28,94]. In LiNRR, a stable triple-phase boundary in GDEs is critical to delivering nitrogen-gas molecules close to the lithium-metal surface. There are several ways to construct GDEs for LiNRR. In one, SSC is used as the GDE substrate[23]. Unlike a conventional carbon-based GDE (for example, carbon cloth/paper), a steel cloth is required for non-aqueous electrolytes, which would otherwise wet the carbon cloth, thus creating a flooded electrode. Lazouski and colleagues used SSC, which has a less favourable surface interaction with the non-aqueous electrolyte compared to carbon cloth/paper, allowing for effective contacting of gas-phase nitrogen with liquid-phase electrolyte throughout the SSC. Application of a pressure gradient further helps in preventing electrolyte flooding, leading to enhanced ammonia production rates[23]. Incorporation of steel-mesh GDEs enhances the ammonia partial current density from 1.3 mA cm^{-2} in flooded electrodes to 8.8 mA cm^{-2} under rate-optimized conditions, as discussed already[23]. Fu and colleagues developed a continuous flow cell with both gas and electrolyte flow capabilities[28]. The combination of an applied pressure gradient across a stainless-steel mesh GDE, along with electrolyte flow using a syringe pump, leads to optimized FEs of 61% at an ammonia partial current density of 3.66 mA cm^{-2}, stable over 700 C of charge passed[28]. Fu and colleagues also observed an impact of GDE mesh size on selectivity, with a 30 µm pore size mesh leading to higher ammonia selectivity than a 5 µm pore size mesh[28].

Cell operating conditions and engineering

The cell types described all operate under a wide range of cell operating conditions. A major limiting factor found for parallel-plate flow cells is their poor nitrogen transport, which autoclave cells and gas diffusion flow cells have been shown to overcome. Pressure is an important operating condition that also impacts nitrogen transport. For example, high FEs are obtained at pressures of 20 bar or higher (Fig. 3), because the partial pressure of nitrogen gas dissolved in the electrolyte is higher[27]. Aside from the operating conditions, cell geometry may also play a factor in reaction selectivity and energy efficiency. Cell designs that decrease the electrode gap can lower the measured overpotential, increasing the cell energy efficiency. Energy efficiency is defined as the fraction of total voltage-driven energy input that is contained in the produced ammonia. Finally, pressure, temperature and overpotential may all impact SEI chemistry, but the effect of changing these operating conditions on the nanoscale SEI remains unexplored. With these factors in mind, commercial LiNRR cells should balance manufacturing complexity with reaction selectivity to reach acceptable economies of scale[95,96].

Future outlook of LiNRR

In this Review we highlight recent developments made in LiNRR, with a focus on the catalytic lithium SEI, kinetic and transport models, accompanying anodic reactions, and cell design considerations. The catalytic SEI is a complex and reactive microstructural environment that we are just beginning to understand. Spectroscopic and chemically selective techniques have revealed the atomic-scale structure and chemical components of the catalytic SEI. These studies have set the foundation for dynamic measurements during electrochemical testing and can help answer important questions. For example, how does the catalytic SEI form, and how does its chemistry and structure change as a function of current density, electrolyte chemistry and time? The development of new in situ characterization methods with sufficient spatial and temporal range will also help answer these questions. Aside from the interfacial characterization of the catalytic SEI, the bulk physical properties of nitrogen in lithium electrolytes remain poorly understood. Quantification of bulk nitrogen transport properties, such as visualization of boundary-layer thicknesses, would help to develop a better understanding of these electrochemical systems

operating under gaseous flow. In parallel, refinement of kinetic and transport models supported by theoretical calculations (using density functional theory, molecular dynamics simulations and so on) will help to accurately capture the chemical and electrochemical complexity of LiNRR. These fundamental studies set the stage for new electrode designs and cell geometries that could further enhance the ammonia FE. Although the lithium-mediated route is one of the few proven viable pathways for ammonia production at reasonable rates and ambient conditions, it faces an intrinsic energy-efficiency limit of ~28% due to the ~3 V driving force needed for lithium reduction. Further strategies grounded in basic science are needed to improve this energy efficiency to approach that of the conventional Haber–Bosch process, which has increased from 36% to 62% over the course of a century of process development. As the world moves towards global decarbonization through electrification, the development and optimization of electrochemical cells producing ammonia near ambient conditions would facilitate carbon-free fertilizer production as an alternative to today's carbon-intensive Haber–Bosch process.

References

1. Jones, K. *The Chemistry of Nitrogen: Pergamon Texts in Inorganic Chemistry* (Elsevier, 2013).
2. Schiffer, Z. J. & Manthiram, K. Electrification and decarbonization of the chemical industry. *Joule* **1**, 10–14 (2017).
3. Foster, S. L. et al. Catalysts for nitrogen reduction to ammonia. *Nat. Catal.* **1**, 490–500 (2018).
4. Hoffman, B. M., Lukoyanov, D., Yang, Z.-Y., Dean, D. R. & Seefeldt, L. C. Mechanism of nitrogen fixation by nitrogenase: the next stage. *Chem. Rev.* **114**, 4041–4062 (2014).
5. Yandulov, D. V. & Schrock, R. R. Catalytic reduction of dinitrogen to ammonia at a single molybdenum center. *Science* **301**, 76–78 (2003).
6. Arashiba, K., Miyake, Y. & Nishibayashi, Y. A molybdenum complex bearing PNP-type pincer ligands leads to the catalytic reduction of dinitrogen into ammonia. *Nat. Chem.* **3**, 120–125 (2011).
7. Kuriyama, S. et al. Catalytic formation of ammonia from molecular dinitrogen by use of dinitrogen-bridged dimolybdenum-dinitrogen complexes bearing PNP-pincer ligands: remarkable effect of substituent at PNP-pincer ligand. *J. Am. Chem. Soc.* **136**, 9719–9731 (2014).
8. Lazouski, N., Schiffer, Z. J., Williams, K. & Manthiram, K. Understanding continuous lithium-mediated electrochemical nitrogen reduction. *Joule* **3**, 1127–1139 (2019).
   Demonstration of LiNRR using a parallel-plate flow cell along with the development of a combined transport-kinetic model for this system.
9. Andersen, S. Z. et al. A rigorous electrochemical ammonia synthesis protocol with quantitative isotope measurements. *Nature* **570**, 504–508 (2019).
   Development of a rigorous quantitative isotope measurement protocol to prevent false-positive ammonia synthesis results.
10. McFarlane, E. F. & Tompkins, F. C. Nitridation of lithium. *Trans. Faraday Soc.* **58**, 997–1007 (1962).
11. Fischer, D., Cancarevic, Z., Schön, J. C. & Jansen, M. Zur Synthese und Struktur von K_3N. *Z. Anorg. Allg. Chem.* **630**, 156–160 (2004).
12. Vajenine, G. V. On reactions between alkali metals and active nitrogen. *Solid State Sci.* **10**, 450–454 (2008).
13. Dey, A. N. Lithium anode film and organic and inorganic electrolyte batteries. *Thin Solid Films* **43**, 131–171 (1977).
14. Peled, E. The electrochemical behavior of alkali and alkaline earth metals in nonaqueous battery systems—the solid electrolyte interphase model. *J. Electrochem. Soc.* **126**, 2047 (1979).
15. Liu, M., Zhang, S., Chen, M. & Wu, L. Boosting electrochemical nitrogen reduction performance through water-in-salt electrolyte. *Appl. Catal. B* **319**, 121925 (2022).
16. Guha, A. et al. Mechanistic insight into high yield electrochemical nitrogen reduction to ammonia using lithium ions. *Mater. Today Commun.* **21**, 100700 (2019).
17. Fichter, F., Girard, P. & Erlenmeyer, H. Elektrolytische bindung von komprimiertem stickstoff bei gewöhnlicher temperatur. *Helv. Chim. Acta* **13**, 1228–1236 (1930).
   First report of lithium metal-mediated nitrogen reduction to ammonia in an autoclave cell at elevated pressures.
18. Tsuneto, A., Kudo, A. & Sakata, T. Efficient electrochemical reduction of N_2 to NH_3 catalyzed by lithium. *Chem. Lett.* **22**, 851–854 (1993).
   First report of Faradaic efficiencies approaching 50% by using tetrahydrofuran (THF) as a non-aqueous electrolyte solvent for LiNRR, at elevated pressure.
19. Tsuneto, A., Kudo, A. & Sakata, T. Lithium-mediated electrochemical reduction of high pressure N_2 to NH_3. *J. Electroanal. Chem.* **367**, 183–188 (1994).
20. McEnaney, J. M. et al. Ammonia synthesis from N_2 and H_2O using a lithium cycling electrification strategy at atmospheric pressure. *Energy Environ. Sci.* **10**, 1621–1630 (2017).
21. Denvir, A., Murphy, O. J., Cisar, A., Robertson, P. & Uselton, K. Electrochemical synthesis of ammonia. US patent 6712950-B2 (2004).
22. Joshi, A. V. & Bhavaraju, S. Ammonia synthesis using lithium ion conductive membrane. US patent 8916123 (2014).
23. Lazouski, N., Chung, M., Williams, K., Gala, M. L. & Manthiram, K. Non-aqueous gas diffusion electrodes for rapid ammonia synthesis from nitrogen and water-splitting-derived hydrogen. *Nat. Catal.* **3**, 463–469 (2020).
   Development of a gas diffusion electrode to overcome nitrogen-transport limitations and enable hydrogen oxidation at the anode, as well as an electrochemical Haber–Bosch reactor coupled to a water electrolyser, thereby producing ammonia from N_2 and H_2O under ambient conditions.
24. Andersen, S. Z. et al. Increasing stability, efficiency and fundamental understanding of lithium-mediated electrochemical nitrogen reduction. *Energy Environ. Sci.* **13**, 4291–4300 (2020).
   Development of a micro-kinetic model for LiNRR and a potential cycling strategy for improved stability.
25. Li, S. et al. Electrosynthesis of ammonia with high selectivity and high rates via engineering of the solid–electrolyte interphase. *Joule* **6**, 2083–2101 (2022).
   High current density of 1 A cm^{-2} through the use of highly porous copper electrodes and the engineering of a compact and uniform SEI.
26. Suryanto, B. H. R. et al. Nitrogen reduction to ammonia at high efficiency and rates based on a phosphonium proton shuttle. *Science* **372**, 1187–1191 (2021).
   Development of a phosphonium proton shuttle to overcome the use of a sacrificial proton source.
27. Du, H.-L. et al. Electroreduction of nitrogen with almost 100% current-to-ammonia efficiency. *Nature* **609**, 722–727 (2022).
   Faradaic efficiency of LiNRR close to 100% by using a high concentration lithium electrolyte salt and tailoring the physicochemical properties of the electrolyte–electrode interface.
28. Fu, X. et al. Continuous-flow electrosynthesis of ammonia by nitrogen reduction and hydrogen oxidation. *Science* **379**, 707–712 (2023).
   Development of a continuous flow cell for ammonia synthesis, a platinum–gold alloy catalyst for hydrogen oxidation at the anode, and achieving a Faradaic efficiency of 61% at ambient conditions with an energy efficiency of 14%.
29. Cui, X., Tang, C. & Zhang, Q. A review of electrocatalytic reduction of dinitrogen to ammonia under ambient conditions. *Adv. Energy Mater.* **8**, 1800369 (2018).

30. Iriawan, H. et al. Methods for nitrogen activation by reduction and oxidation. *Nat. Rev. Methods Prim.* **1**, 56 (2021).
31. Tang, C. & Qiao, S.-Z. How to explore ambient electrocatalytic nitrogen reduction reliably and insightfully. *Chem. Soc. Rev.* **48**, 3166–3180 (2019).
32. Westhead, O. et al. Near ambient N_2 fixation on solid electrodes versus enzymes and homogeneous catalysts. *Nat. Rev. Chem.* **7**, 184–201 (2023).
33. Yu, W., Lewis, N. S., Gray, H. B. & Dalleska, N. F. Isotopically selective quantification by UPLC-MS of aqueous ammonia at submicromolar concentrations using dansyl chloride derivatization. *ACS Energy Lett.* **5**, 1532–1536 (2020).
34. Nielander, A. C. et al. A versatile method for ammonia detection in a range of relevant electrolytes via direct nuclear magnetic resonance techniques. *ACS Catal.* **9**, 5797–5802 (2019).
35. Choi, J. et al. Identification and elimination of false positives in electrochemical nitrogen reduction studies. *Nat. Commun.* **11**, 5546 (2020).
36. Zaffaroni, R., Ripepi, D., Middelkoop, J. & Mulder, F. M. Gas chromatographic method for in situ ammonia quantification at parts per billion levels. *ACS Energy Lett.* **5**, 3773–3777 (2020).
37. Cai, X. et al. Interaction of ammonia with nafion and electrolyte in electrocatalytic nitrogen reduction study. *J. Phys. Chem. Lett.* **12**, 6861–6866 (2021).
38. Verdouw, H., Van Echteld, C. J. A. & Dekkers, E. M. J. Ammonia determination based on indophenol formation with sodium salicylate. *Water Res.* **12**, 399–402 (1978).
39. Giner-Sanz, J. J., Leverick, G., Pérez-Herranz, V. & Shao-Horn, Y. Optimization of the salicylate method for ammonia quantification from nitrogen electroreduction. *J. Electroanal. Chem.* **896**, 115250 (2021).
40. Giner-Sanz, J. J., Leverick, G. M., Pérez-Herranz, V. & Shao-Horn, Y. Salicylate method for ammonia quantification in nitrogen electroreduction experiments: the correction of iron III interference. *J. Electrochem. Soc.* **167**, 134519 (2020).
41. Giner-Sanz, J. J., Leverick, G. M., Giordano, L., Pérez-Herranz, V. & Shao-Horn, Y. Alkali metal salt interference on the salicylate method for quantifying ammonia from nitrogen reduction. *ECS Adv.* **1**, 024501 (2022).
42. Krempl, K. et al. Quantitative operando detection of electro synthesized ammonia using mass spectrometry. *ChemElectroChem* **9**, e202101713 (2022).
43. Kibsgaard, J., Nørskov, J. K. & Chorkendorff, I. The difficulty of proving electrochemical ammonia synthesis. *ACS Energy Lett.* **4**, 2986–2988 (2019).
44. Cherepanov, P. V., Krebsz, M., Hodgetts, R. Y., Simonov, A. N. & MacFarlane, D. R. Understanding the factors determining the faradaic efficiency and rate of the lithium redox-mediated N_2 reduction to ammonia. *J. Phys. Chem. C* **125**, 11402–11410 (2021).
45. Lin, B., Wiesner, T. & Malmali, M. Performance of a small-scale Haber process: a techno-economic analysis. *ACS Sustain. Chem. Eng.* **8**, 15517–15531 (2020).
46. Vojvodic, A. et al. Exploring the limits: a low-pressure, low-temperature Haber–Bosch process. *Chem. Phys. Lett.* **598**, 108–112 (2014).
47. Peled, E. Film forming reaction at the lithium/electrolyte interface. *J. Power Sources* **9**, 253–266 (1983).
48. Peled, E. & Menkin, S. SEI: past, present and future. *J. Electrochem. Soc.* **164**, A1703 (2017).
49. Xu, K. Nonaqueous liquid electrolytes for lithium-based rechargeable batteries. *Chem. Rev.* **104**, 4303–4417 (2004).
50. Goodenough, J. B. & Kim, Y. Challenges for rechargeable Li batteries. *Chem. Mater.* **22**, 587–603 (2010).
51. Winter, M., Barnett, B. & Xu, K. Before Li ion batteries. *Chem. Rev.* **118**, 11433–11456 (2018).
52. Xu, K. Electrolytes and interphases in Li-ion batteries and beyond. *Chem. Rev.* **114**, 11503–11618 (2014).
53. Xu, K. *Electrolytes, Interfaces and Interphases* (Royal Society of Chemistry, 2023).
54. Aurbach, D. et al. Design of electrolyte solutions for Li and Li-ion batteries: a review. *Electrochim. Acta* **50**, 247–254 (2004).
55. Hobold, G. M. et al. Moving beyond 99.9% Coulombic efficiency for lithium anodes in liquid electrolytes. *Nat. Energy* **6**, 951–960 (2021).
56. Steinberg, K. et al. Imaging of nitrogen fixation at lithium solid electrolyte interphases via cryo-electron microscopy. *Nat. Energy* **8**, 138–148 (2022).
57. Kanamura, K., Tamura, H., Shiraishi, S. & Takehara, Z. XPS analysis of lithium surfaces following immersion in various solvents containing $LiBF_4$. *J. Electrochem. Soc.* **142**, 340–347 (1995).
58. Wang, C., Meng, Y. S. & Xu, K. Perspective—fluorinating interphases. *J. Electrochem. Soc.* **166**, A5184–A5186 (2019).
59. Chang, W., Park, J. H., Dutta, N. S. & Arnold, C. B. Morphological and chemical mapping of columnar lithium metal. *Chem. Mater.* **32**, 2803–2814 (2020).
60. Li, Y. et al. Atomic structure of sensitive battery materials and interfaces revealed by cryo-electron microscopy. *Science* **358**, 506–510 (2017).
61. Li, K. et al. Enhancement of lithium-mediated ammonia synthesis by addition of oxygen. *Science* **374**, 1593–1597 (2021).
62. Westhead, O. et al. The role of ion solvation in lithium mediated nitrogen reduction. *J. Mater. Chem. A Mater. Energy Sustain.* **11**, 12746–12758 (2023).
63. Westhead, O. et al. The origin of overpotential in lithium-mediated nitrogen reduction. *Faraday Discuss.* **243**, 321–338 (2023).
64. Sažinas, R. et al. Towards understanding of electrolyte degradation in lithium-mediated non-aqueous electrochemical ammonia synthesis with gas chromatography-mass spectrometry. *RSC Adv.* **11**, 31487–31498 (2021).
65. Schwalbe, J. A. et al. A combined theory-experiment analysis of the surface species in lithium-mediated NH_3 electrosynthesis. *ChemElectroChem* **7**, 1542–1549 (2020).
66. Aurbach, D. et al. Recent studies on the correlation between surface chemistry, morphology, three-dimensional structures and performance of Li and Li-C intercalation anodes in several important electrolyte systems. *J. Power Sources* **68**, 91–98 (1997).
67. Sažinas, R. et al. Oxygen-enhanced chemical stability of lithium-mediated electrochemical ammonia synthesis. *J. Phys. Chem. Lett.* **13**, 4605–4611 (2022).
68. Aurbach, D., Daroux, M. L., Faguy, P. W. & Yeager, E. Identification of surface films formed on lithium in dimethoxyethane and tetrahydrofuran solutions. *J. Electrochem. Soc.* **135**, 1863 (1988).
69. Wang, E., Dey, S., Liu, T., Menkin, S. & Grey, C. P. Effects of atmospheric gases on Li metal cyclability and solid-electrolyte interphase formation. *ACS Energy Lett.* **5**, 1088–1094 (2020).
70. Spry, M. et al. Water increases the Faradaic selectivity of Li-mediated nitrogen reduction. *ACS Energy Lett.* **8**, 1230–1235 (2023).
71. Cai, X. et al. Lithium-mediated electrochemical nitrogen reduction: mechanistic insights to enhance performance. *iScience* **24**, 103105 (2021).
72. Furukawa, T. & Hirakawa, Y. Basic experiment on lithium removal technique. In *Proc. 2012 20th International Conference on Nuclear Engineering and the ASME 2012 Power Conference* 9–13 (2013).
73. Lazouski, N. et al. Proton donors induce a differential transport effect for selectivity toward ammonia in lithium-mediated nitrogen reduction. *ACS Catal.* **12**, 5197–5208 (2022).
74. Zhou, F. et al. Electro-synthesis of ammonia from nitrogen at ambient temperature and pressure in ionic liquids. *Energy Environ. Sci.* **10**, 2516–2520 (2017).

75. Pecher, O., Carretero-González, J., Griffith, K. J. & Grey, C. P. Materials' methods: NMR in battery research. *Chem. Mater.* **29**, 213–242 (2017).
76. Moshkovich, M., Gofer, Y. & Aurbach, D. Investigation of the electrochemical windows of aprotic alkali metal (Li, Na, K) salt solutions. *J. Electrochem. Soc.* **148**, E155 (2001).
77. Blair, S. J. et al. Lithium-mediated electrochemical nitrogen reduction: tracking electrode-electrolyte interfaces via time-resolved neutron reflectometry. *ACS Energy Lett.* **7**, 1939–1946 (2022).
78. Gibanel, F., López, M. C., Royo, F. M., Santafé, J. & Urieta, J. S. Solubility of nonpolar gases in tetrahydrofuran at 0 to 30 °C and 101.33 kPa partial pressure of gas. *J. Solut. Chem.* **22**, 211–217 (1993).
79. Kang, C. S. M., Zhang, X. & MacFarlane, D. R. Synthesis and physicochemical properties of fluorinated ionic liquids with high nitrogen gas solubility. *J. Phys. Chem. C* **122**, 24550–24558 (2018).
80. Kang, C. S. M., Zhang, X. & MacFarlane, D. R. High nitrogen gas solubility and physicochemical properties of [C_4mpyr][eFAP]-fluorinated solvent mixtures. *J. Phys. Chem. C* **123**, 21376–21385 (2019).
81. Littel, R. J., Versteeg, G. F. & Van Swaaij, W. P. M. Diffusivity measurements in some organic solvents by a gas-liquid diaphragm cell. *J. Chem. Eng. Data* **37**, 42–45 (1992).
82. Clark, E. L. et al. Standards and protocols for data acquisition and reporting for studies of the electrochemical reduction of carbon dioxide. *ACS Catal.* **8**, 6560–6570 (2018).
83. Wang, Y., Rogers, E. I. & Compton, R. G. The measurement of the diffusion coefficients of ferrocene and ferrocenium and their temperature dependence in acetonitrile using double potential step microdisk electrode chronoamperometry. *J. Electroanal. Chem.* **648**, 15–19 (2010).
84. Bard, A. J. & Faulkner, L. R. *Electrochemical Methods* (Wiley, 2011).
85. Singh, A. R. et al. Strategies toward selective electrochemical ammonia synthesis. *ACS Catal.* **9**, 8316–8324 (2019).
86. Kim, K., Chen, Y., Han, J.-I., Yoon, H. C. & Li, W. Lithium-mediated ammonia synthesis from water and nitrogen: a membrane-free approach enabled by an immiscible aqueous/organic hybrid electrolyte system. *Green Chem.* **21**, 3839–3845 (2019).
87. Du, H.-L. et al. The chemistry of proton carriers in high-performance lithium-mediated ammonia electrosynthesis. *Energy Environ. Sci.* **16**, 1082–1090 (2023).
88. Kim, K. et al. Electrochemical synthesis of ammonia from water and nitrogen: a lithium-mediated approach using lithium-ion conducting glass ceramics. *ChemSusChem* **11**, 120–124 (2018).
89. Krempl, K., Pedersen, J. B., Kibsgaard, J., Vesborg, P. C. K. & Chorkendorff, I. Electrolyte acidification from anode reactions during lithium mediated ammonia synthesis. *Electrochem. Commun.* **134**, 107186 (2022).
90. Hodgetts, R. Y., Du, H.-L., Nguyen, T. D., MacFarlane, D. & Simonov, A. N. Electrocatalytic oxidation of hydrogen as an anode reaction for the Li-mediated N_2 reduction to ammonia. *ACS Catal.* **12**, 5231–5246 (2022).
91. Lobaccaro, P. et al. Effects of temperature and gas–liquid mass transfer on the operation of small electrochemical cells for the quantitative evaluation of CO_2 reduction electrocatalysts. *Phys. Chem. Chem. Phys.* **18**, 26777–26785 (2016).
92. Becker, R., Weber, K., Pfeiffer, T. V., van Kranendonk, J. & Schouten, K. J. A scalable high-throughput deposition and screening setup relevant to industrial electrocatalysis. *Catalysts* **10**, 1165 (2020).
93. Maljuric, S., Jud, W., Kappe, C. O. & Cantillo, D. Translating batch electrochemistry to single-pass continuous flow conditions: an organic chemist's guide. *J. Flow Chem.* **10**, 181–190 (2020).
94. Higgins, D., Hahn, C., Xiang, C., Jaramillo, T. F. & Weber, A. Z. Gas-diffusion electrodes for carbon dioxide reduction: a new paradigm. *ACS Energy Lett.* **4**, 317–324 (2019).
95. Gomez, J. R. & Garzon, F. Preliminary economics for green ammonia synthesis via lithium mediated pathway. *Int. J. Energy Res.* **45**, 13461–13470 (2021).
96. Lazouski, N. et al. Cost and performance targets for fully electrochemical ammonia production under flexible operation. *ACS Energy Lett.* **7**, 2627–2633 (2022).
97. Li, K. et al. Increasing current density of Li-mediated ammonia synthesis with high surface area copper electrodes. *ACS Energy Lett.* **7**, 36–41 (2021).
98. Tort, R. et al. Nonaqueous Li-mediated nitrogen reduction: taking control of potentials. *ACS Energy Lett.* **8**, 1003–1009 (2023).
99. LiNRR: meta-analysis of LiNRR literature (GitHub); https://github.com/Manthiram-Group/LiNRR

Acknowledgements

This material is based on work supported by the National Science Foundation (grant no. 2204756). We gratefully acknowledge support from the Resnick Sustainability Institute. K.M. gratefully acknowledges support from the Sloan Foundation. W.C. acknowledges funding support from the Arnold and Mabel Beckman Foundation via a 2022 Arnold O. Beckman Postdoctoral Fellowship in Chemical Sciences. F.R. acknowledges funding support from the Independent Research Fund Denmark (DFF), case no. 0217-00234B. We also thank M. Yusov, C. Klein and G. Lee for productive and helpful feedback and discussions.

Author contributions

W.C. conducted the initial meta-analysis from literature sources, analysed the data and generated the figures. A.J. brought the manuscript to submission-ready completion with detailed edits. W.C. and A.J. led the majority of the work, with input from the whole group. F.R. helped decide our cell-naming convention. K.M. mentored, edited and financed the work. All authors contributed to manuscript proofreading.

Competing interests

The authors declare no competing interests.

Additional information

Correspondence and requests for materials should be addressed to Karthish Manthiram.

Peer review information *Nature Catalysis* thanks Hoang-Long Du and the other, anonymous, reviewer for their contribution to the peer review of this work.